Cooper pair splitting and recombination in a nanoSQUID geometry at high transparency

R. Jacquet,[1] J. Rech,[1] T. Jonckheere,[1] A. Zazunov,[2] and T. Martin[1]

[1]*Aix-Marseille Université, Université de Toulon, CNRS, CPT, UMR 7332, 13288 Marseille, France*
[2]*Institut für Theoretische Physik IV, Heinrich Heine Universität, D-40225 Düsseldorf, Germany*

We describe a Josephson device composed of two superconductors separated by two interacting quantum dots in parallel, where clear manifestations of Cooper pair splitting and subsequent recombination occur. Indeed, in addition to sequential tunneling of electrons through each dot, an additional transport channel exists in this system: crossed Andreev reflection, where a Cooper pair from the source is split between the two dots and recombined in the drain superconductor. Unlike nonequilibrium scenarios for Cooper pair splitting which involve superconducting/normal metal "forks", our proposal relies on an Aharonov-Bohm measurement of the DC Josephson current when a flux is inserted between the two dots. We provide a path integral approach to treat arbitrary transparencies, and we explore all contributions for the individual phases (0 or π) of the quantum dots. We propose a definition of the Cooper pair splitting efficiency (the fraction of the electron transfer processes which involve the splitting of a Cooper pair) for arbitrary transparencies, which allows us to find the phase associations which favor the crossed Andreev process. Possible applications to experiments using nanowires as quantum dots are discussed.

　　　　PACS number(s): 74.50.+r, 85.25.Dq, 73.21.La

I. INTRODUCTION

The ground state of a superconductor is described by the BCS wave function, where electrons form Cooper pairs [1]. If for some reason a pair exits the superconductor, its constituent electrons can be transmitted in a normal metal conductor: a process called (reverse) Andreev reflection, where a hole from the normal metal incident on the superconductor is converted as a reflected electron in this same metal. If the superconductor is connected to two such metallic contacts whose separation is smaller than the superconducting coherence length, a hole incident from the first contact can be reflected as an electron in the second contact. This process is called crossed Andreev reflection (CAR) and corresponds to Cooper pair splitting: A Cooper pair exits the superconductor, and its two constituent electrons propagate in two different metallic leads.

The initial manifestation of CAR was proposed theoretically for nonlocal current [2–6], as well as for nonequilibrium noise cross correlations (current-current fluctuations between the superconductor and the two outgoing devices) [7–14], which have a positive sign if the CAR process is favored. CAR can also occur for a superconductor connected to two quantum dots in the Coulomb blockade regime: If the dots can only accommodate one electron at a time, a Cooper pair can be split between the two dots [15,16].

On the experimental side, attention has mainly focused on nonlocal current measurement on the Cooper pair beam splitter [17], a device where typically the superconducting source of electrons is connected to two leads, sometimes via embedded quantum dots [18–21]. Under specific gate voltages imposed on such dots, it is possible to trigger electronic transport in the two outgoing conductors. Only a single experiment managed to measure positive noise cross correlations when the source of electrons was rendered superconducting [22].

The main challenge with these experiments resides in the fact that they rely on nonequilibrium measurements. Strictly speaking, Refs. [18–21] constitute indirect evidence of Cooper pair splitting, as opposed to noise cross-correlation measurements. The latter represent a considerable ordeal due to the poor signal to noise ratio, and no attempt has been made so far to reproduce the results of Ref. [22].

A seminal theoretical work has been suggested early on to circumvent these difficulties by proposing a Josephson equilibrium current geometry to test Cooper pair splitting [23]. It describes two superconductors (with applied phase difference) separated by two quantum dots [24] placed in parallel. When a Cooper pair is transmitted from one superconductor to the other, the two electrons can either pass both through a given dot, or they can transit through different dots (cf. Fig. 1). This indeed realizes an Aharonov-Bohm (AB) experiment with superconductors as source and drain, driven by an applied phase difference. The critical current as a function of the AB flux should be π periodic if electrons are not split between the two dots and 2π periodic if Cooper pair splitting is effective. The clear originality of this proposal resides in the fact that unlike nonequilibrium noise setups, here Cooper pair splitting is uncovered using a current measurement at equilibrium albeit in a Josephson geometry. The calculation was performed perturbatively in the tunneling Hamiltonian, with infinite repulsion on the dots. Dot gate voltages insured that on average each dot was occupied by a single electron. A complementary study appeared a decade later with the same setup [25], and perturbative results for dot levels which were assumed to be above the superconducting chemical potentials and with a finite Coulomb repulsion were also presented.

First, so far no analysis of this superconducting Aharonov-Bohm effect has allowed us to go beyond lowest order perturbation theory in the tunneling Hamiltonian. Advances in superconducting device fabrication [26] seem to indicate that by burying nanowires underneath superconductors, large transmission can be achieved between the resulting quantum dot and the lead. Treating the tunnel coupling to all orders of perturbation theory thus constitutes a first motivation of our study.

Secondly, it is established that when a quantum dot is embedded in a Josephson junction, away from the Kondo
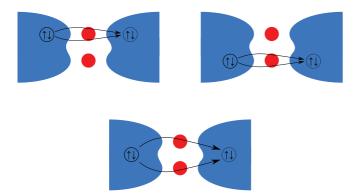
FIG. 1. (Color online) Illustration of the three different possibilities for the transmission of a Cooper pair from the left superconductor to the right one. The two electrons of the pair can either be both transmitted through the upper dot (top left), through the lower dot (top right), or the Cooper pair can be split with one electron transmitted through each dot (bottom).

regime, the strength of the on-site repulsion, the coupling to the leads, and the level position of the dot determine whether it constitutes a 0 or a π junction (positive or negative Josephson amplitude). This has been analyzed perturbatively [27], as well as with path integral formalism, followed by a saddle point approximation [28]. This latter work allows us to distinguish between three phases of the Josephson junction: (a) the π phase (where the dot is singly occupied), (b) the $0^{(0)}$ phase (where it is unoccupied), and (c) the $0^{(2)}$ phase (with double occupation). These predictions have been verified experimentally a decade ago [29]. In the Josephson setup with two dots in parallel, which is studied here, each dot can be in either the $0^{(0)}$, the $0^{(2)}$, or the π phase. In Ref. [23] the two electrons are both in a π junction configuration, while Ref. [25] has also considered the case where both dots are in the $0^{(0)}$ phase. However, there is to date no systematic or comparative study specifying which combination of the dot phases may enhance or reduce the AB signal for maximal observation, even less so for arbitrarily large transparencies.

The two above points constitute the main motivations of the present paper. In this paper, we employ the path integral formalism to model the AB setup without any restrictions on the transmission properties of the sample. Indeed, we provide results both in the tunneling and the high transparency regimes, and we propose a way to measure the efficiency of CAR processes in both cases, by analyzing the AB signal. We find that the CAR processes are optimized when the two quantum dots are in the same phase.

CAR processes are also intimately related to entanglement, which constitutes yet another motivation for perfecting our understanding of such processes. Indeed, when the two electrons of a Cooper pair are separated in two different normal metal electrodes, one expects that the entanglement of the spin degrees of freedom is preserved because the tunneling processes are spin-preserving. CAR processes thus create spatially separated entangled electron pairs. Tests of quantum entanglement, based on Bell inequality violation measurements, could be implemented via noise cross correlations with the so-called superconducting Cooper pair splitter [30,31]. Moreover, these ideas have been applied to the paradigm of

quantum teleportation [32,33], as well as in other applications [34,35].

The paper is organized as follows. In Sec. II we provide a description of the device and of the model with which we describe it, and we give an expression of the partition function in terms of Grassmann variables. The free energy used to derive the Josephson current of this nanoSQUID in a nonperturbative manner is presented in Sec. III. In Sec. IV, we discuss the possible occupancy states of the dots. We propose the definition of a Cooper pair splitting efficiency in Sec. V which can be computed for arbitrary transparencies of the studied junctions. The AB signals are calculated first in the tunneling regime in Sec. VI and then in the nonperturbative regime in Sec. VII, and all possible phase associations for the dots are considered. In Sec. VIII, we propose a few natural extensions to our work and discuss our results in Sec. IX.

II. MODEL AND PARTITION FUNCTION

The device is illustrated in Fig. 2. For simplicity, the two leads consist of the same superconducting material with a controllable phase difference which can either be imposed by closing the device in a loop geometry or embedding the device in a macroscopic SQUID [23,25]. Two quantum dots are placed in parallel in the nanogap between the two electrodes, and a magnetic flux (which is in principle independent from the one imposed to trigger a DC Josephson signal between the electrodes) threads the area between the two dots. Electrons can tunnel from the source electrode to the upper or lower dot, but on-site Coulomb repulsion favors zero or single occupation on the latter. In the presence of a magnetic flux between the two dots, because of the AB effect, different phase shifts are expected between the two paths that an electron can follow to reach the drain electrode. If the separation between injection points is larger than the coherence length, Cooper pairs as a whole pass either by the upper or lower path, as in Ref. [26]. If the injection points are closer together than the superconducting coherence length however, the two electrons of the pair can travel through opposite dots, realizing a CAR process on this first superconductor, followed by an "inverse" CAR process on the second superconductor, giving another contribution to the Josephson current (see Fig. 1). By adjusting the quantum dot energy levels and Coulomb interaction, we expect to filter the electrons and eventually favor the CAR process. Note however that this setup does not allow us to
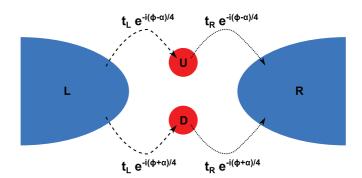

FIG. 2. (Color online) Path dependent phase shifts.

extract direct information on the degree of entanglement of the dot electrons due to these CAR processes.

We denote by $\hat{d}^{\dagger}_{a\sigma}$ the creation operator for an electron with spin $\sigma = \uparrow,\downarrow$ on the quantum dot $a = U, D$ and by $\hat{\psi}^{\dagger}_{jk\sigma}$ the creation operator for an electron with momentum k and spin $\sigma = \uparrow,\downarrow$ in the superconductor $j = L, R$. It is convenient to introduce the Nambu spinors

$$\hat{d}_a = \begin{pmatrix} \hat{d}_{a\uparrow} \\ \hat{d}^{\dagger}_{a\downarrow} \end{pmatrix} \quad \text{and} \quad \hat{\psi}_{jk} = \begin{pmatrix} \hat{\psi}_{jk,\uparrow} \\ \hat{\psi}^{\dagger}_{j(-k),\downarrow} \end{pmatrix}. \quad (1)$$

σ_i $(i = x,y,z)$ are the Pauli matrices that act in Nambu space. The Hamiltonian of the double Josephson junction reads

$$\mathcal{H} = \sum_{a=U,D} H_a + \sum_{j=L,R} H_j + H_t. \quad (2)$$

H_a is the Hamiltonian of the quantum dot $a = U, D$, characterized by its energy level ε_a and its on-site Coulomb repulsion U_a:

$$H_a = \varepsilon_a \sum_{\sigma=\uparrow,\downarrow} \hat{d}^{\dagger}_{a\sigma} \hat{d}_{a\sigma} + U_a \hat{n}_{a\uparrow} \hat{n}_{a\downarrow}, \quad (3)$$

with $\hat{n}_{a\sigma} = \hat{d}^{\dagger}_{a\sigma} \hat{d}_{a\sigma}$ the dot occupation operator per spin. H_j is the Hamiltonian of the superconductor $j = L, R$, with gap Δ and chemical potential μ:

$$H_j = \sum_k \hat{\psi}^{\dagger}_{jk}(\xi_k \sigma_z + \Delta \sigma_x)\hat{\psi}_{jk}, \quad \xi_k = \frac{k^2}{2m} - \mu. \quad (4)$$

Here Δ is real; the phase difference between electrodes has been gauged out and instead appears in the tunneling Hamiltonian. If we denote by $\mathbf{r}_{ja}$ the location of the injection point from lead j to dot a, the tunneling Hamiltonian H_t reads

$$H_t = \sum_{jka} e^{i\mathbf{k}\cdot\mathbf{r}_{ja}} \hat{\psi}^{\dagger}_{jk} \mathcal{T}_{ja} \hat{d}_a + \text{H.c.} \quad (5)$$

The tunneling matrices involved in Eq. (5) read

$$\mathcal{T}_{LU} = t_L \sigma_z e^{+i\frac{\phi-\alpha}{4}\sigma_z}, \quad \mathcal{T}_{RU} = t_R \sigma_z e^{-i\frac{\phi-\alpha}{4}\sigma_z}, \quad (6a)$$

$$\mathcal{T}_{LD} = t_L \sigma_z e^{+i\frac{\phi+\alpha}{4}\sigma_z}, \quad \mathcal{T}_{RD} = t_R \sigma_z e^{-i\frac{\phi+\alpha}{4}\sigma_z}. \quad (6b)$$

ϕ is the phase difference between the superconductors, while α is related to the magnetic flux Φ inside the SQUID loop: $\alpha = 2\pi \frac{\Phi}{\Phi_0}$ where $\Phi_0 = h/e$ is the flux quantum. For clarity, the phase shifts acquired by tunneling electrons are indicated in Fig. 2.

We employ a path integral approach in the Matsubara formalism in order to compute the partition function of the device. We introduce then the eigenvalues of the annihilation operators $\hat{\psi}_{jk\sigma}$ and $\hat{d}_{a\sigma}$ written as $\psi_{jk\sigma}$ and $d_{a\sigma}$, respectively. These are Grassmann variables, and we consider also their conjugates $\overline{\psi}_{jk\sigma}$ and $\overline{d}_{a\sigma}$ as well as the collections in Nambu spinors d_a and ψ_{jk} defined in the same way as Eq. (1). The partition function is given by a functional integration over paths that are β antiperiodic:

$$Z = \int_{\substack{d_a(\beta) = -d_a(0) \\ \psi_{jk}(\beta) = -\psi_{jk}(0)}} \mathcal{D}[\overline{d},d,\overline{\psi},\psi] \exp[-S_E(\overline{d},d,\overline{\psi},\psi)]. \quad (7)$$

The Euclidean action S_E reads

$$S_E(\overline{d},d,\overline{\psi},\psi) = \int_0^{\beta} d\tau \left\{ \mathcal{H}(\overline{d},d,\overline{\psi},\psi) \right.$$
$$\left. + \sum_a \overline{d}_a \partial_\tau d_a + \sum_{jk} \overline{\psi}_{jk} \partial_\tau \psi_{jk} \right\}, \quad (8)$$

where the matrix elements of the Hamiltonian can be written as

$$\mathcal{H}(\overline{d},d,\overline{\psi},\psi) = \sum_a H_a(\overline{d}_a,d_a) + \sum_{jk} H_{jk}(\overline{\psi}_{jk},\psi_{jk})$$
$$+ \sum_{jka} H_{t,jka}(\overline{d}_a,d_a,\overline{\psi}_{jk},\psi_{jk}). \quad (9)$$

The expressions of H_{jk} and $H_{t,jka}$ are readily obtained from Eqs. (4) and (5) by substituting the annihilation operators $\hat{a}$ by their eigenvalues a and the corresponding creation operators $a^{\dagger}$ by the conjugate Grassmann variables $\overline{a}$. For the quantum dots, we can also find an expression in terms of Nambu spinors as follows:

$$H_a(\overline{d}_a,d_a) = \tilde{\varepsilon}_a + \tilde{\varepsilon}_a \overline{d}_a \sigma_z d_a - \frac{U_a}{2}(\overline{d}_a d_a)^2, \quad (10)$$

with $\tilde{\varepsilon}_a = \varepsilon_a + \frac{U_a}{2}$.

III. FREE ENERGY AND JOSEPHSON CURRENT

As the lead degrees of freedom are quadratic in the Hamiltonian, they can be easily integrated out. The partition function is then expressed as a functional integral over the dot Grassmann variables:

$$Z = c_1 \int_{d_a(\beta)=-d_a(0)} \prod_a \mathcal{D}[\overline{d}_a,d_a] \exp[-S_{\text{eff}}(\overline{d},d)], \quad (11)$$

where c_1 is the determinant arising from the integration of the lead variables, which is independent of ϕ and α. The effective action in Eq. (11) reads

$$S_{\text{eff}}(\overline{d},d) = \sum_a \int_0^{\beta} d\tau \left\{ \tilde{\varepsilon}_a + \overline{d}_a(\tau)[\partial_\tau \mathbb{1}_2 + \tilde{\varepsilon}_a \sigma_z]d_a(\tau) \right.$$
$$\left. - \frac{U_a}{2}(\overline{d}_a(\tau) d_a(\tau))^2 \right\}$$
$$- \sum_{a,b} \int_0^{\beta} d\tau \int_0^{\beta} d\tau' \, \overline{d}_a(\tau) \Sigma^{ab}(\tau - \tau') d_b(\tau'), \quad (12)$$

where the self-energy term

$$\Sigma^{ab}(\tau) = \sum_{jk} e^{i\mathbf{k}\cdot(\mathbf{r}_{jb}-\mathbf{r}_{ja})} \mathcal{T}^{\dagger}_{ja} G_k(\tau) \mathcal{T}_{jb} \quad (13)$$

involves the Green function of the leads $G_k(\tau)$, which verifies

$$[\partial_\tau \mathbb{1}_2 + \xi_k \sigma_z + \Delta \sigma_x]G_k(\tau) = \delta(\tau)\mathbb{1}_2. \quad (14)$$

The quartic terms $(\overline{d}_a d_a)^2$ in Eq. (12) prohibit an exact computation of the partition function. As in Ref. [28], we use a Hubbard-Stratonovich transformation to treat these terms, and we neglect the temporal fluctuations of the two auxiliary

fields X_U and X_D which are introduced:

$$e^{\frac{U_a}{2} \int_0^\beta d\tau (\bar{d}_a d_a)^2} \approx \sqrt{\frac{\beta}{2\pi U_a}} \int_{-\infty}^{+\infty} dX_a \, e^{-\frac{\beta}{2U_a} X_a^2 + X_a \int_0^\beta d\tau \, \bar{d}_a d_a}.$$

(15)

Because both the Green's functions G_k and the Nambu spinor components $d_{a\sigma}$ are β antiperiodic, we use a Matsubara series expansion $F(\tau) = \sum_{p \in \mathbb{Z}} e^{-i\omega_p \tau} F(\omega_p)$ over the frequencies

$\omega_p = (p + \frac{1}{2})2\pi/\beta$. Rather than keeping track of a cumbersome device-specific position dependence of the self-energy, we choose to introduce a phenomenological parameter η. It extrapolates between the two most relevant cases: $\eta = 0$ for infinitely distant injection points (much more separated than the superconducting coherence length) and $\eta = 1$ for coinciding injection points (much closer than the superconducting coherence length). The dots are now integrated out and the partition function becomes

$$Z^\eta(\phi,\alpha) = c_1 c_2 \int_{-\infty}^{+\infty} dX_U \int_{-\infty}^{+\infty} dX_D \exp\left[-S_{\text{eff}}^{\text{HS},\eta}(X_U, X_D, \phi, \alpha) \right],$$

(16)

where c_2 is a fermionic determinant arising from the dot variables integration. The effective action reads

$$S_{\text{eff}}^{\text{HS},\eta}(X_U, X_D, \phi, \alpha) = \sum_a \left(\beta \tilde{\varepsilon}_a + \frac{\beta}{2U_a} X_a^2 \right) - 2 \sum_{p \in \mathbb{N}} \ln\left(\beta^4 \left| \det\left[\mathcal{M}_p^\eta(X_U, X_D, \phi, \alpha) \right] \right| \right),$$

(17)

$$\mathcal{M}_p^\eta(X_U, X_D, \phi, \alpha) = \begin{bmatrix} -(i\omega_p + X_U)\mathbb{1}_2 + \tilde{\varepsilon}_U \sigma_z - \mathcal{A}_p(\phi - \alpha) & -\mathcal{B}_p^\eta(\phi, +\alpha) \\ -\mathcal{B}_p^\eta(\phi, -\alpha) & -(i\omega_p + X_D)\mathbb{1}_2 + \tilde{\varepsilon}_D \sigma_z - \mathcal{A}_p(\phi + \alpha) \end{bmatrix},$$

(18)

$$\mathcal{A}_p(\phi) = \frac{\Gamma}{\sqrt{\Delta^2 + \omega_p^2}} \left[i\omega_p \mathbb{1}_2 - \Delta\left(\cos\frac{\phi}{2} \sigma_x + \gamma \sin\frac{\phi}{2} \sigma_y \right) \right],$$

(19)

$$\mathcal{B}_p^\eta(\phi, \alpha) = \eta \frac{\Gamma}{\sqrt{\Delta^2 + \omega_p^2}} \left[i\omega_p \left(\cos\frac{\alpha}{2} \mathbb{1}_2 + i\gamma \sin\frac{\alpha}{2} \sigma_z \right) - \Delta\left(\cos\frac{\phi}{2} \sigma_x + \gamma \sin\frac{\phi}{2} \sigma_y \right) \right].$$

(20)

The decay rate is defined as $\Gamma = \pi \nu(0)(t_L^2 + t_R^2)$, where $\nu(0)$ is the density of states of the leads at the Fermi level. The contact asymmetry is given by $\gamma = (t_L^2 - t_R^2)/(t_L^2 + t_R^2)$.

The CAR process is due to the off-diagonal terms $\mathcal{B}_p$ of the matrices $\mathcal{M}_p$, the determinants of which we have to compute as a result of the Gaussian integrals over quantum dot degrees of freedom. In practice, these off-diagonal terms depend on the separation between injection points $R \equiv |\mathbf{r}_{jU} - \mathbf{r}_{jD}|$. They have an exponential decay on the scale of the superconducting coherence length. With the microscopic tunneling Hamiltonian formulation of Eq. (5), they also bear fast oscillations on the Fermi wavelength and possibly power law decay depending on the dimensionality $[\eta(R) = (\sin k_F R)/(k_F R)$ for 3D superconductors [23,36] and no power law decay for quasi-one-dimensional superconductors [37]]. Existing CAR experiments [18–21] based on nanowire quantum dots embedded in the superconducting leads are typically performed for an injection separation which is less than the superconducting coherence length. Yet these experiments find no evidence of either Fermi wavelength oscillations or power law decay at all: The nonlocal signal is strong and can be optimized by tuning the dot gate voltages. This can be attributed to the proximity effect from the bulk superconductors, which acts on the nanowires used in the experiments. To keep our discussion more general, and avoid such device-specific complications, in this paper we use η as a phenomenological parameter, as in Refs. [25,38]. Most of the results will be displayed for the extreme values $\eta = 0$ and $\eta = 1$, but in order to show the evolution of the AB signals, we sometimes allow it to vary smoothly between these two values.

To evaluate the partition function of Eq. (16), we use a saddle-point method [28]. The effective action

$S_{\text{eff}}^{\text{HS},\eta}(X_U, X_D, \phi, \alpha)$ is computed numerically by summing over Matsubara frequencies (up to a cutoff much larger than the superconducting gap). Its minimum, located in $[X_U^*(\phi,\alpha), X_D^*(\phi,\alpha)]$, is obtained with a gradient descent method for fixed ϕ and α (the number of starting points of the algorithm depends on the symmetry of the function to be minimized). The free energy is then defined from this minimum value as $S_{\text{eff}}^{\text{HS},\eta}(X_U^*(\phi,\alpha), X_D^*(\phi,\alpha), \phi, \alpha) \equiv \beta F^\eta(\phi,\alpha)$. The current is finally obtained by differentiating the free energy with respect to the phase difference ϕ:

$$J^\eta(\phi,\alpha) = 2 \, \partial_\phi F^\eta(\phi,\alpha).$$

(21)

The critical current, function of the flux α, is defined as

$$J_c^\eta(\alpha) = \max_\phi |J^\eta(\phi,\alpha)|.$$

(22)

For $\eta = 0$, it is π periodic. Indeed, in this case, there are no CAR processes, and for a magnetic flux α, the current characteristic (current as a function of the phase difference ϕ) through the double junction is simply the sum of the current characteristics across the independent single junctions, one being shifted by $-\alpha$ and the other one by $+\alpha$. Shifting α by π results in adding a phase shift $-\pi$ for one of the two junctions $[\mathcal{A}_p(\phi - \alpha) \to \mathcal{A}_p(\phi - \alpha - \pi)$ in the top left block of Eq. (18)] and a phase shift $+\pi$ for the other one $[\mathcal{A}_p(\phi + \alpha) \to \mathcal{A}_p(\phi + \alpha + \pi)$ in the bottom right block of Eq. (18)]. Because of the 2π periodicity in ϕ of the current through a single junction, the critical current of the double junction is unchanged when $\alpha \to \alpha + \pi$. This is in contrast to the case with $\eta = 1$, i.e., in the presence of CAR processes, where the off-diagonal terms of Eq. (18) imply that only the 2π periodicity of the critical current can be observed.

IV. 0-π TRANSITION IN A SINGLE JOSEPHSON JUNCTION

As a first step, let us recall some known results concerning a single dot embedded in a Josephson junction. In this section, we summarize the properties of such a setup, and we determine under what condition the junction is in the $0^{(0)}$, the π, or the $0^{(2)}$ phase. The 0 phase is characterized by a positive Josephson current for $\phi \in [0,\pi]$. It can be further separated between a $0^{(0)}$ phase where the dot is almost empty and a $0^{(2)}$ phase where the mean occupation number of the dot is almost 2. The π phase is associated with a negative Josephson current for $\phi \in [0,\pi]$ and corresponds to a singly occupied dot.

In perturbative calculations, the Josephson current flowing through the quantum dot is the result of the tunneling of Cooper pairs, which requires a fourth order perturbative expansion in the tunneling amplitudes between a superconductor and the quantum dot. At this order, the current can be written as $J = J_0 \sin \phi$, where ϕ is the phase difference between the superconductors, and the sign of J_0 determines the 0 or π character of the junction. Providing a single occupancy on the quantum dot ($0 < -\varepsilon \ll U$) J_0 can be negative [27] unlike the case of an empty quantum dot.

This phenomenon has been investigated numerically [28] for arbitrary transmissions between the dot and the superconducting leads. For a fixed quantum dot energy level $\varepsilon < 0$ and a fixed decay rate Γ, the current as a function of the phase difference ϕ between the superconductors undergoes a discontinuity as one tunes the Coulomb interaction U across a critical value. Computing the mean occupation number on the quantum dot in the $(-\varepsilon, U)$ plane reveals the presence of all three phases, as shown in Fig. 3, where the π phase, which lies around the line $2\varepsilon + U = 0$, separates the $0^{(0)}$ and $0^{(2)}$ phases.

V. SPLITTING EFFICIENCY

In order to identify the optimal regime for observing signatures of CAR processes in the AB signal, we need to define a splitting efficiency: a way to quantify contributions to
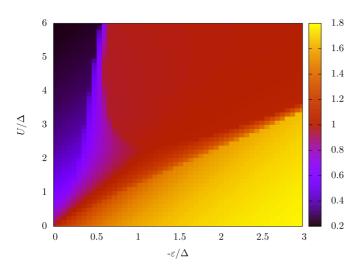

FIG. 3. (Color online) Mean occupation number diagram of the quantum dot of a single Josephson junction for symmetric couplings ($t_L = t_R$) and for $\Gamma = \Delta$, $\beta = 50\Delta^{-1}$.

the Josephson current involving Cooper pair splitting. We start by discussing the case of low electron transmission, where intuition can be gained from simple perturbation theory. We then aim at comparing the results of our general approach for arbitrary transmission to the perturbative results for the AB signal.

The fourth order perturbation expansion [23,25] in the tunneling amplitudes t_j allows us to write the Josephson current as three contributions, associated with the three different processes illustrated in Fig. 1, so that

$$J(\phi,\alpha) = I_D \sin(\phi + \alpha) + I_U \sin(\phi - \alpha) + I_{CAR} \sin \phi.$$
(23)

Indeed, in the presence of a magnetic flux $\alpha \neq 0$, an additional phase shift is acquired, depending on the path that each electron of the Cooper pair followed between the two superconducting leads. When the Cooper pair tunnels through the U (resp. D) quantum dot, it accumulates a phase shift $-\alpha$ (resp. $+\alpha$) in addition to the superconducting phase difference and contributes to the Josephson current with an amplitude I_U (resp. I_D). However, when the Cooper pair is delocalized on the two quantum dots (via the CAR process, thus contributing with an amplitude I_{CAR}), one electron gets a phase shift $+\frac{\alpha}{2}$ while the other one gets a phase shift $-\frac{\alpha}{2}$, the pair accumulating as a result no additional phase shift.

The critical current associated with the Josephson current Eq. (23) then reads

$$J_c(\alpha) = I_0 \sqrt{1 + a \cos \alpha + b \cos 2\alpha}$$
(24)

with $I_0 = \sqrt{I_U^2 + I_D^2 + I_{CAR}^2}$, $I_0^2 a = 2I_{CAR}(I_U + I_D)$, and $I_0^2 b = 2I_D I_U$. For low enough values of Γ, we are in the tunneling regime, and the approximation Eq. (23) for the Josephson current is justified. If we are able to extract the parameters I_U, I_D, and I_{CAR}, e.g., from a fit of the AB signal, we can calculate the quantity

$$r_t = \frac{I_{CAR}^2}{I_U^2 + I_D^2 + I_{CAR}^2},$$
(25)

which encodes the splitting efficiency of the double Josephson junction. It varies between 0 and 1. $r_t = 0$ corresponds to a low efficiency of the CAR process, while $r_t = 1$ is obtained when this process of spatial delocalization of the two electrons of a Cooper pair is much more important than the tunneling processes of a whole Cooper pair through a single quantum dot.

As already stressed, the formalism developed in Secs. II and III is valid regardless of the strength of the coupling between the superconductors and the quantum dots. However, the above definition of the splitting efficiency relies on the expression Eq. (24) for the critical current which is no longer valid in the nonperturbative regime. There, one needs an alternative diagnosis for the detection of the CAR process. As it turns out, a relevant quantity can be extracted from the mean powers of the critical current obtained for infinitely distant injection points ($\eta = 0$) and for coinciding ones ($\eta = 1$). Indeed,
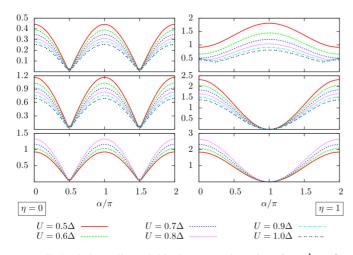
FIG. 4. (Color online) Critical current (in units of $10^{-4}e\Delta/\hbar$) curves for symmetric associations of dots in the tunneling regime: π-π (top panel), $0^{(0)}$-$0^{(0)}$ (middle panel), $0^{(2)}$-$0^{(2)}$ (bottom panel).

defining $\mathcal{P}_\eta = \int_0^{2\pi} d\alpha \, [J_c^\eta(\alpha)]^2$, we compute the quantity

$$r = \frac{|\mathcal{P}_{\eta=1} - \mathcal{P}_{\eta=0}|}{\mathcal{P}_{\eta=1}}. \qquad (26)$$

This generalizes the concept of splitting efficiency to the case of arbitrary transmission and coincides with the definition of Eq. (25) in the tunneling regime.

VI. NANOSQUID IN THE TUNNELING REGIME

We first focus on the tunneling regime, taking a low value of the decay rate $\Gamma = 0.01\Delta$. We choose to explore all the possible combinations for the phases of the two quantum dots (see Figs. 4 and 5). The results were obtained for symmetric couplings $\gamma = 0$ at temperature $\beta^{-1} = 0.002\Delta$. The energies of the quantum dots are: $\varepsilon = -0.3\Delta$ for the π phase, $\varepsilon = 0.3\Delta$ for the $0^{(0)}$ phase, and $\varepsilon = -0.9\Delta$ for the $0^{(2)}$ phase. The Coulomb interaction U is chosen to be the same for the two
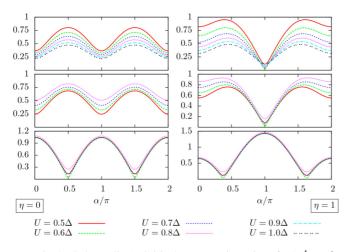

FIG. 5. (Color online) Critical current (in units of $10^{-4}e\Delta/\hbar$) curves for asymmetric associations of dots in the tunneling regime: π-$0^{(0)}$ (top panel), π-$0^{(2)}$ (middle panel), $0^{(0)}$-$0^{(2)}$ (bottom panel).

quantum dots and within a specific range, as staying in a given phase at fixed energy restricts the possible values for U.

The particle-hole symmetry ensures that the current is invariant under the change $(\tilde{\varepsilon}_U, \tilde{\varepsilon}_D) \rightarrow (-\tilde{\varepsilon}_U, -\tilde{\varepsilon}_D)$. For the values of energy ε mentioned above, this implies that the critical current is identical for $0^{(0)}$-$0^{(0)}$ and $0^{(2)}$-$0^{(2)}$ phase associations with $U = 0.6\Delta$, for π-$0^{(0)}$ and π-$0^{(2)}$ phase associations again with $U = 0.6\Delta$, and finally for $0^{(0)}$-$0^{(0)}$ at $U = 0.7\Delta$ and $0^{(2)}$-$0^{(2)}$ at $U = 0.5\Delta$.

We first consider the critical current curves of a SQUID made of two independent single Josephson junctions, i.e., for $\eta = 0$. In this particular case, $I_{CAR} = 0$ and consequently $a = 0$ in Eq. (24), so that the extrema of the critical current are the zeros of $\sin 2\alpha$, and the total Josephson current is given by Eq. (23) with $I_{CAR} = 0$. From the results of Figs. 4 and 5, it clearly appears that there is a $\pi/2$ phase shift in the critical current between the situation where the two dots are in the same phase (0-0 or π-π) and the one where they are in different phases (π-0). More specifically, for two quantum dots in the same phase ($I_D I_U > 0$), there is no phase shift between the currents of the two single Josephson junctions for $\alpha = 0$, so that the maxima are added ($|I_D + I_U| = |I_D| + |I_U|$) and, as a result, the critical current is maximal for $\alpha = 0$. However, for two quantum dots in different phases ($I_D I_U < 0$), the phase shift of π between the currents of the two single Josephson junctions for $\alpha = 0$ is compensated by a phase shift $\alpha = +\pi/2$ for one of the currents and a phase shift $-\alpha = -\pi/2$ for the other one ($|I_D - I_U| = |I_D| + |I_U|$) resulting in a maximum of the critical current for $\alpha = \pi/2$. Such behavior has been observed experimentally [26].

Comparing the left panels of Figs. 4 and 5 to the right ones (i.e., the case $\eta = 0$ to $\eta = 1$), we immediately obtain evidence of the crosstalk between the two single Josephson junctions: The period of the critical current doubles. This is a signature of the emergence of the CAR process. Note that the symmetric associations (cf. Fig. 4) differ completely between $\eta = 0$ and $\eta = 1$: For the π-π association, the maximum at $\alpha = 0$ for $\eta = 0$ becomes a minimum for $\eta = 1$, and for the $0^{(0)}$-$0^{(0)}$ and $0^{(2)}$-$0^{(2)}$ associations, the maximum at $\alpha = \pi$ for $\eta = 0$ becomes a zero for $\eta = 1$. Concerning the asymmetric associations (cf. Fig. 5), the critical current curves for $\eta = 1$ somehow look like those obtained for $\eta = 0$: The positions of the maxima and minima are mostly preserved for all phase associations; only their local or global character changes when tuning η.

Increasing U results in a more pronounced filtering as the processes where the quantum dots are doubly occupied are less favored. This explains the observed decrease in critical current for the $0^{(0)}$-$0^{(0)}$ and π-π associations (Fig. 4). The opposite behavior happens when the quantum dots are doubly occupied, i.e., for the $0^{(2)}$-$0^{(2)}$ association. There, increasing U favors processes where the occupation of the dots is lowered, since approaching the π transition results in the decrease of the mean occupation number on the quantum dot. Such opposite behaviors while tuning U for $0^{(0)}$-$0^{(0)}$ and $0^{(2)}$-$0^{(2)}$ phase associations can be seen as a consequence of the already discussed particle-hole symmetry. Similarly, the π-$0^{(0)}$ and π-$0^{(2)}$ combinations have opposite interaction dependence (see Fig. 5). Interestingly, the interaction has no noticeable effect in the case of the $0^{(0)}$-$0^{(2)}$ phase association.
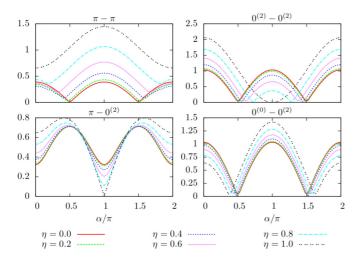
FIG. 6. (Color online) Influence of the parameter η on the critical current (in units of $10^{-4} e\Delta/\hbar$) in the tunneling regime ($U = 0.6\Delta$).

In order to monitor the emergence of CAR processes, we investigate intermediate regimes in Fig. 6 for the π-π, $0^{(2)}$-$0^{(2)}$, π-$0^{(2)}$, and $0^{(0)}$-$0^{(2)}$ phase associations by turning on η progressively from 0 to 1. This is a phenomenological way to introduce more and more CAR processes, as the injection points in the superconductors are brought together, from $\eta = 0$ (no CAR effect) to $\eta = 1$ (maximal CAR effect). We observe a dramatic increase of the critical current in the symmetric configurations (π-π and $0^{(2)}$-$0^{(2)}$ phase associations), while in the asymmetric configurations (π-$0^{(2)}$ and $0^{(0)}$-$0^{(2)}$ phase associations), the modification of the AB signal is noticeable but not substantial.

We display the splitting efficiency r given by Eq. (26) for all phase associations in Fig. 7. In the studied domain for Coulomb repulsion parameter U, we do not observe noticeable evolutions of r except for the $0^{(0)}$-π association for which we see a clear decrease. The symmetric associations of phases (for which the critical current differs the most between $\eta = 0$ and $\eta = 1$) lead to the highest values of r. The highest splitting efficiency is obtained for two quantum dots in the
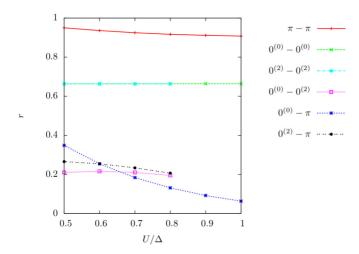
π phase: Ensuring a mean occupation number around 1 on each quantum dot favors the CAR process. One can get some insight concerning the value of r for the associations $0^{(0)}$-$0^{(0)}$ and $0^{(2)}$-$0^{(2)}$ from the perturbative calculation presented in the previous section. Indeed, in the tunneling regime the splitting efficiency r matches the definition r_t of Eq. (25) in terms of the amplitudes I_D, I_U, and I_{CAR}. For symmetric associations, we must add the constraint $I_D = I_U \equiv I/2$ to the fit procedure, so that the critical current reads

$$\frac{J_c(\alpha)}{|I|} = \left| \frac{I_{CAR}}{I} + \cos\alpha \right|, \tag{27}$$

and since the critical current in symmetric associations of 0 phases vanishes for $\alpha = \pi$, we get $I_{CAR}/I = 1$ and $r_t = 2/3$.

VII. NANOSQUID IN THE HIGH TRANSPARENCY REGIME

The advantage of the formalism developed in Secs. II and III relies on the possibility to address high transparency regimes of the double Josephson junction under study. The results presented in this section are obtained for symmetric couplings $\gamma = 0$ at temperature $\beta^{-1} = 0.02\Delta$ and for a decay rate $\Gamma = 2\Delta$. The energies of the quantum dots are: $\varepsilon = -4\Delta$ for the π phase, $\varepsilon = 4\Delta$ for the $0^{(0)}$ phase, and $\varepsilon = -12\Delta$ for the $0^{(2)}$ phase. Particle-hole symmetry implies that the critical current is identical for $0^{(0)}$-$0^{(0)}$ and $0^{(2)}$-$0^{(2)}$ phase associations with $U = 8\Delta$, for π-$0^{(0)}$ and π-$0^{(2)}$ phase associations again with $U = 8\Delta$, and finally for $0^{(0)}$-$0^{(0)}$ at $U = 9\Delta$ and $0^{(2)}$-$0^{(2)}$ at $U = 7\Delta$.

The strategy is again to investigate all the possible combinations of phases for the quantum dots (which correspond to different mean occupation numbers) in order to reproduce the qualitative study of Sec. VI. Our goal is to determine what features are preserved and what has changed and to compute the splitting efficiency r defined by Eq. (26) in order to determine which associations of phases favor nonlocal phenomena the most. The critical current curves are given in Figs. 8 and 9.
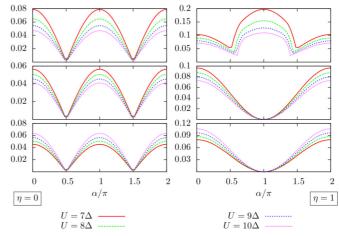

FIG. 7. (Color online) Splitting efficiency r given by Eq. (26) extracted from the curves of Figs. 4 and 5.

FIG. 8. (Color online) Critical current (in units of $e\Delta/\hbar$) curves for symmetric associations of dots in the high transparency regime: π-π (top panel), $0^{(0)}$-$0^{(0)}$ (middle panel), $0^{(2)}$-$0^{(2)}$ (bottom panel).
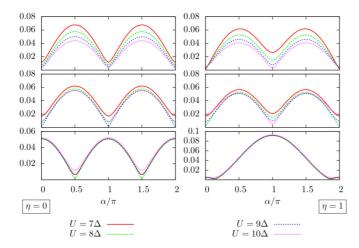
FIG. 9. (Color online) Critical current (in units of $e\Delta/\hbar$) curves for asymmetric associations of dots in the high transparency regime: π-$0^{(0)}$ (top panel), π-$0^{(2)}$ (middle panel), $0^{(0)}$-$0^{(2)}$ (bottom panel).

FIG. 10. (Color online) Influence of the parameter η on the critical current (in units of $e\Delta/\hbar$) in the high transparency regime ($U = 8\Delta$).

From the results of the π-π association for $\eta = 1$, it is clear that we are no longer in the tunneling regime as the flux dependence cannot be fitted by Eq. (24) together with the constraint that $I_D = I_U$. We can again notice, for $\eta = 0$, the $\pi/2$ phase shift in the critical current between dots in the π-0 phases (top and middle panels of Fig. 9) and dots in the 0-0 or π-π phases (Fig. 8 and bottom panel of Fig. 9).

The critical current in Figs. 8 and 9 again presents a doubling of its period when switching η from 0 to 1. This is due to the emergence of nonlocal processes where both quantum dots are involved. For the π-π association, during this switching, $\alpha = 0$ remains a local maximum (contrary to the tunneling regime). For $0^{(0)}$-$0^{(0)}$ and $0^{(2)}$-$0^{(2)}$ phase associations, the maximum at $\alpha = \pi$ for $\eta = 0$ becomes a zero for $\eta = 1$ (as in the tunneling regime). There is little influence (less than in the tunneling regime) of η on the π-$0^{(2)}$ and π-$0^{(0)}$ associations, whereas for the $0^{(0)}$-$0^{(2)}$ association the maximum in $\alpha = 0$ is considerably lowered (more than in the tunneling regime) from $\eta = 0$ to $\eta = 1$.

For symmetric associations of phases, the evolution of the critical current with increasing U (Fig. 8) can be explained following the same arguments as in the tunneling regime. While the filtering of electrons tunneling through $0^{(0)}$ or π quantum dots is responsible for a decrease of the signal, favoring one-electron processes through a $0^{(2)}$ quantum dot results in an increase of the signal. The opposite U dependence for the $0^{(0)}$-$0^{(0)}$ and $0^{(2)}$-$0^{(2)}$ phase associations is a consequence of particle-hole symmetry. While there is still no noticeable effect of U on the $0^{(0)}$-$0^{(2)}$ association as in the tunneling regime, the π-$0^{(2)}$ association also shows little U dependence. As a consequence, we do not observe the opposite behavior as a function of U for the π-$0^{(0)}$ and π-$0^{(2)}$ associations (Fig. 9).

We introduce progressively nonlocal effects in Fig. 10 by switching η from 0 to 1. For the symmetric associations (π-π and $0^{(2)} - 0^{(2)}$) as well as for the $0^{(0)}$-$0^{(2)}$ configuration (contrary to the tunneling regime), the AB signal is dramatically increased when CAR processes are switched on. On the contrary, the π-$0^{(2)}$ phase association is hardly influenced by the presence of nonlocal processes (even less than in the tunneling regime). We can quantify the importance of CAR
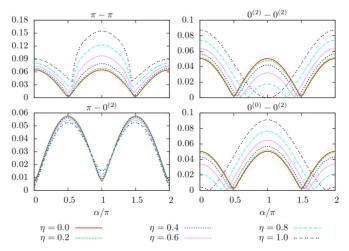
processes compared to the direct tunneling through a single quantum dot by calculating the splitting efficiency r given by Eq. (26), which we display in Fig. 11 for the different associations of phases. As a function of U, the splitting efficiencies which are found are essentially constant over the range considered. As it turns out, although we work with specific phases for the individual quantum dots, implying specific populations, the quantization of the electron charge on these dots is ineffective at high transparencies because they constitute "open quantum dots" involving large fluctuations from their average population. This is consistent with the observation that the splitting efficiency varies little with U. As mentioned above, there is little influence of η on the π-$0^{(2)}$ and π-$0^{(0)}$ associations, and this is why these are the lowest splitting efficiencies we found. The splitting efficiencies of the associations of 0 phases are around 0.55, and the highest splitting efficiency is still obtained for the π-π association.

Finally, we note that the energy levels of the dots can be easily varied experimentally using electrostatic gates. Varying
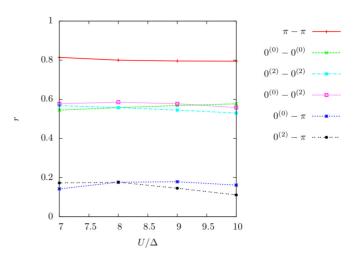

FIG. 11. (Color online) Splitting efficiency r given by Eq. (26) extracted from the curves of Figs. 8 and 9.
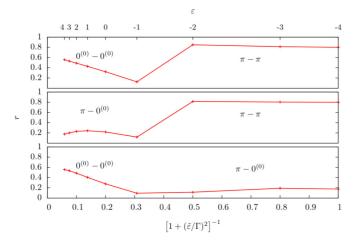
FIG. 12. (Color online) Evolution of the splitting efficiency as a function of the effective transparency $D(\varepsilon)$ [Eq. (28)] for fixed $\Gamma = 2\Delta$ and $U = 8\Delta$. Top: The energy levels of both dots are taken to be identical and varied simultaneously ($\varepsilon_U = \varepsilon_D \equiv \varepsilon$). Middle: the D quantum dot is taken in the π phase ($\varepsilon_D = -4\Delta$), while the energy of the U dot is varied ($\varepsilon_U \equiv \varepsilon$). Bottom: the D quantum dot is taken in the $0^{(0)}$ phase ($\varepsilon_D = 4\Delta$), while the energy of the U dot is varied ($\varepsilon_U \equiv \varepsilon$).

the position of the energy level ε of a quantum dot at fixed decay rate Γ and fixed Coulomb on-site repulsion U changes the effective transparency defined as

$$D(\varepsilon) = \frac{\Gamma^2}{\Gamma^2 + \left(\varepsilon + \frac{U}{2}\right)^2}. \tag{28}$$

Thus, by varying the energy levels of the two dots, we can optimize the splitting efficiency by reaching the π-π phase at high effective transparency. We show in the top panel of Fig. 12 the splitting efficiency as a function of the energy level of the two dots, taken to be identical. The abrupt change of the efficiency near $D(\varepsilon) = 0.4$ shows the crossover from the $0^{(0)}$-$0^{(0)}$ to the π-π junction. Similarly, when tuning only one of the two energy levels, while maintaining the other dot in the π (middle panel) or the $0^{(0)}$ phase (bottom panel), the splitting efficiency shows a marked transition as a function of the effective transparency.

VIII. EXTENSIONS AND PERSPECTIVES

Several directions can be envisioned beyond the mean-field approximation presented here. In this section, we explore three possible extensions of the present work, both from a purely theoretical standpoint and from the point of view of observing the presented results experimentally.

The present project relies on a Hubbard-Stratonovich treatment of the Coulomb interactions on the quantum dots involving auxiliary fields, which is of course exact if the path integral over the latter is performed. In principle, this allows us to access the Kondo regime for the quantum dots if the fluctuations of the auxiliary fields around the saddle point approximation are fully taken into account. For Josephson junctions containing a single quantum dot, the Kondo regime, where the Kondo temperature $T_K = \sqrt{\Gamma U}/2 \, e^{\pi \varepsilon_0(\varepsilon_0 + U)/(\Gamma U)}$ [39] exceeds the superconducting gap Δ, has been reached

either with a Hubbard Stratonovich transformation approach followed by a Monte Carlo numerical treatment of the auxiliary field [40] or by an exact numerical renormalization group approach [41]. For these single dot Josephson junctions, the Kondo regime imposes a 0 phase with high harmonics describing the current phase relationship. The present work is therefore restricted to the regime where $T_K < \Delta$. Within the range of parameters chosen in our numerical study, we find that the Kondo temperature is at most $T_K = 0.13\Delta$, which gives us confidence in our working assumptions. Nevertheless, extensions of this work could be envisioned by going beyond the saddle point approximation of the Hubbard Stratonovich transformation for the double dot junctions. In a first step, Gaussian fluctuations around the saddle point approximation could be included in order to improve our solution, but only a full Monte Carlo numerical treatment of the auxiliary fields would allow us to reach the Kondo regime of this double dot Josephson junction. Alternatively, a numerical renormalization group method [41] could be employed. At any rate, when working under the assumption $T_K > \Delta$, the Kondo regime could be avoided altogether by working with dot gate voltages such that only the $0^{(0)}$-$0^{(0)}$ combination of phases occurs (zero average occupation on both dots). According to Fig. 11 this combination of phases still has a sizable splitting efficiency.

Given the relative complexity of the device, and for the sake of simplicity, we have chosen to ignore here the effects of both direct interdot tunneling and interdot Coulomb interaction. In our previous work on superconducting/normal metal forks, Ref. [11], we addressed the issue of interdot tunneling and found that the pair splitting signal (positive noise crossed correlations) can be spoiled when interdot tunneling becomes too large (of the order of the dot-electrode tunneling). We expect the same effect on the present device, which means that all the results presented in this paper should remain valid in the presence of interdot tunneling as long as it is smaller than the other tunnel couplings. Coulomb interactions between the dots are likely to render the operation of our device in the π-π phase (our optimal candidate for large splitting efficiency) less efficient, because they disfavor the presence of one electron on each dot. They should not have substantial consequences on the other combination of phases. Granted, the generalization of this work to include the effect of interdot tunneling or interdot Coulomb interaction does not present important technical difficulties, as these effects can in principle be incorporated in our Hubbard Stratonovich scheme, yet such extensions go beyond the scope of this paper.

Finally, a limitation of the present Cooper pair diagnosis resides in the fact that the nanoSQUID requires reduced dimensions so that the injection points to the dots on both superconductors are separated by a distance smaller than the coherence length. This imposes constraints on the separation of the quantum dots, and as a consequence, the area where the AB flux is imposed becomes reduced. Recall that in order to perform the AB diagnosis, a few flux quanta need to be introduced in this area, but if the imposed magnetic field needed to apply several flux quanta becomes larger than the critical field of the superconductors, the whole diagnosis breaks down. In order to optimize the surface area encompassed between the dots, we believe the best choice would be to work with nanowire/nanotube quantum dots,
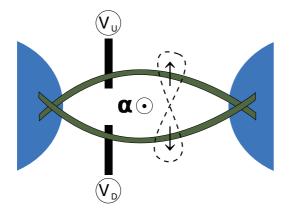
FIG. 13. (Color online) Setup with nanowire/nanotube quantum dots.

which have a large aspect ratio, and which nevertheless can achieve large charging energies even though their length may exceed several μm [42]. This possibility is illustrated in Fig. 13. To work out the numbers, we find that imposing two magnetic flux quanta within a 1 μm^2 area requires a magnetic field of 8×10^{-3} T, which is still smaller than the critical field of superconducting materials such as aluminum (10^{-2} T) or niobium (0.2 T). Note that aluminum could be quite adapted due to its long coherence length (1.6 μm).

IX. CONCLUSION

We have studied a double Josephson junction consisting of two quantum dots connected to two superconductors as a tool to probe Cooper pair splitting. When the two single Josephson junctions which constitute our device are coupled to each other via CAR processes, the doubling of the period of the critical current measured in a nanoSQUID experiment provides proof that Cooper pair splitting and recombination operates and is evidence for the emergence of nonlocal phenomena in the electronic transport of the double junction. This type of diagnosis may prove more convenient than nonequilibrium scenarios involving a superconducting source of electrons and two normal leads/dots where either nonlocal conductance signal or noise cross correlations are measured. While this setup does not provide direct proof of entanglement of the dot electrons, it is clear that this phenomenon plays an essential role.

While this device had been studied in the context of perturbation theory in the tunneling Hamiltonian coupling the dot to the leads [23,25], to our knowledge no generalization to arbitrary transmission had been proposed, and no systematic study for optimizing the CAR signal with respect to the phases $(0^{(0)}, \pi, 0^{(2)})$ of the quantum dots had been attempted. The path integral approach of Ref. [28], within reasonable

approximations (saddle point treatment), allows us to meet these goals. One of the key results of the present paper resides in defining the degree of efficiency of Cooper pair splitting and evaluating it for the different dot configurations.

We first studied the tunneling regime where the usual perturbative expression for the Josephson signal allows us to fit our numerical results and to introduce a natural definition of the splitting efficiency. We were also able to generalize this quantity to arbitrary transparency, providing a criterion for the efficiency of CAR processes which is based on an analysis of the AB signal of the Josephson critical current. We thus studied the prominence of nonlocal phenomena depending on the phases of the quantum dots and found that the π-π association optimizes the splitting of the Cooper pairs that are emitted from one superconductor and recombined on the other one. Yet, our analysis shows that the $0^{(0)}$-$0^{(0)}$ and $0^{(2)}$-$0^{(2)}$ combinations also provide robust Cooper pair splitting signals. Within each of these combinations of phases, we see for the most part that variations of the Coulomb repulsion parameter have little influence on the Cooper pair splitting efficiency.

Furthermore, we treated the CAR coupling parameter η in a phenomenological manner (varying it between 0 and 1), justifiably so because so far no experimental investigation of Cooper pair splitting in superconducting–normal metal "forks" out of equilibrium seems to find the power law suppression which is attributed to bulk 3D superconductors. This may be due to the fact that microscopic models have to be revisited, taking into account that electron emission/absorption in the superconductors is not pointlike but should be averaged over some finite volume, reducing the effect of oscillations over the Fermi wavelength of the CAR parameter.

Recently, we became aware of a current biased measurement [43] which studies precisely the behavior of the double dot Josephson junction. There, a (remarkable) comparative study of the switching current (the current required to transit to the dissipative regime with voltage bias) was performed for different dot phase configurations. This experiment seems to provide realistic evidence of Cooper pair splitting, albeit indirectly, because the self-organized quantum dots embedded in the Josephson junction are too close in order to impose the necessary magnetic flux to observe the AB oscillations.

[1] J. Bardeen, L. N. Cooper, and J. R. Schrieffer, Phys. Rev. **108**, 1175 (1957).

[2] J. M. Byers and M. E. Flatté, Phys. Rev. Lett. **74**, 306 (1995).

[3] G. Deutscher and D. Feinberg, Appl. Phys. Lett. **76**, 487 (2000).

[4] R. Mélin and D. Feinberg, Eur. Phys. J. B **26**, 101 (2002); R. Mélin and S. Peysson, Phys. Rev. B **68**, 174515 (2003); R. Mélin and D. Feinberg, *ibid.* **70**, 174509 (2004); R. Mélin, *ibid.* **72**, 054503 (2005); S. Duhot and R. Mélin, *ibid.* **77**, 014525 (2008).

[5] D. Feinberg, Eur. Phys. J. B **36**, 419 (2003).

[6] D. S. Golubev and A. D. Zaikin, Phys. Rev. B **82**, 134508 (2010); M. S. Kalenkov and A. D. Zaikin, JETP Lett. **87**, 140 (2008) [Pis'ma v ZhETF **87**, 166 (2008)].

[7] M. P. Anantram and S. Datta, Phys. Rev. B **53**, 16390 (1996).

[8] T. Martin, Phys. Lett. A **220**, 137 (1996).

[9] J. Torrès and T. Martin, Eur. Phys. J. B **12**, 319 (1999).

[10] G. B. Lesovik, T. Martin, and G. Blatter, Eur. Phys. J. B **24**, 287 (2001).

[11] D. Chevallier, J. Rech, T. Jonckheere, and T. Martin, Phys. Rev. B **83**, 125421 (2011).

[12] J. Rech, D. Chevallier, T. Jonckheere, and T. Martin, Phys. Rev. B **85**, 035419 (2012).

[13] C. Bena, S. Vishveshwara, L. Balents, and M. P. A. Fisher, Phys. Rev. Lett. **89**, 037901 (2002).

[14] V. Bouchiat, N. Chtchelkatchev, D. Feinberg, G. B. Lesovik, T. Martin, and J. Torrès, Nanotechnol. **14**, 77 (2003).

[15] P. Recher, E. V. Sukhorukov, and D. Loss, Phys. Rev. B **63**, 165314 (2001).

[16] O. Sauret, D. Feinberg, and T. Martin, Phys. Rev. B **70**, 245313 (2004).

[17] D. Beckmann, H. B. Weber, and H. v. Löhneysen, Phys. Rev. Lett. **93**, 197003 (2004).

[18] L. Hofstetter, S. Csonka, J. Nygård, and C. Schönenberger, Nature (London) **461**, 960 (2009).

[19] L. G. Herrmann, F. Portier, P. Roche, A. Levy Yeyati, T. Kontos, and C. Strunk, Phys. Rev. Lett. **104**, 026801 (2010).

[20] J. Schindele, A. Baumgartner, and C. Schönenberger, Phys. Rev. Lett. **109**, 157002 (2012).

[21] L. Hofstetter, S. Csonka, A. Baumgartner, G. Fülöp, S. d'Hollosy, J. Nygård, and C. Schönenberger, Phys. Rev. Lett. **107**, 136801 (2011).

[22] A. Das, Y. Ronen, M. Heiblum, D. Mahalu, A. V. Kretinin, and H. Shtrikman, Nat. Commun. **3**, 1165 (2012).

[23] M.-S. Choi, C. Bruder, and D. Loss, Phys. Rev. B **62**, 13569 (2000).

[24] A. Martín-Rodero and A. Levy Yeyati, Adv. Phys. **60**, 899 (2011).

[25] Z. Wang and X. Hu, Phys. Rev. Lett. **106**, 037002 (2011).

[26] J.-P. Cleuziou, W. Wernsdorfer, V. Bouchiat, T. Ondarçuhu, and M. Monthioux, Nat. Nanotechnol. **1**, 53 (2006).

[27] S. A. Kivelson and B. Z. Spivak, Phys. Rev. B **45**, 10490 (1992).

[28] A. V. Rozhkov and D. P. Arovas, Phys. Rev. Lett. **82**, 2788 (1999).

[29] J. A. van Dam, Y. V. Nazarov, E. P. A. M. Bakkers, S. De Franceschi, and L. P. Kouwenhoven, Nature (London) **442**, 667 (2006).

[30] N. M. Chtchelkatchev, G. Blatter, G. B. Lesovik, and T. Martin, Phys. Rev. B **66**, 161320(R) (2002).

[31] O. Sauret, T. Martin, and D. Feinberg, Phys. Rev. B **72**, 024544 (2005).

[32] O. Sauret, D. Feinberg, and T. Martin, Eur. Phys. J. B **32**, 545 (2003).

[33] O. Sauret, D. Feinberg, and T. Martin, Phys. Rev. B **69**, 035332 (2004).

[34] C. Bennet and D. DiVincenzo, Nature (London) **404**, 247 (2000).

[35] R. Ursin, F. Tiefenbacher, T. Schmitt-Manderbach, H. Weier, T. Scheidl, M. Lindenthal, B. Blauensteiner, T. Jennewein, J. Perdigues, P. Trojek, B. Omer, M. Furst, M. Meyenburg, J. Rarity, Z. Sodnik, C. Barbieri, H. Weinfurter, and A. Zeilinger, Nat. Phys. **3**, 481 (2007).

[36] A. Popoff, Ph.D. thesis, Université de la Méditerranée - Aix-Marseille II, 2008.

[37] J. Rech, T. Jonckheere, T. Martin, B. Douçot, D. Feinberg, and R. Mélin, Phys. Rev. B **90**, 075419 (2014).

[38] I. A. Sadovskyy, G. B. Lesovik, G. Blatter, T. Jonckheere, and T. Martin, Phys. Rev. B **85**, 125442 (2012).

[39] W. G. van der Wiel, S. De Franceschi, T. Fujisawa, J. M. Elzerman, S. Tarucha, and L. P. Kouwenhoven, Science **289**, 2105 (2000).

[40] F. Siano and R. Egger, Phys. Rev. Lett. **93**, 047002 (2004).

[41] M.-S. Choi, M. Lee, K. Kang, and W. Belzig, Phys. Rev. B **70**, 020502(R) (2004).

[42] S. J. Tans, A. R. M. Verschueren, and C. Dekker, Nature (London) **393**, 49 (1998).

[43] R. S. Deacon, A. Oiwa, J. Sailer, S. Baba, Y. Kanai, K. Shibata, K. Hirakawa, and S. Tarucha, Nat. Commun. **6**, 7446 (2015).